Mesoporous Carbon Materials

International Edition: DOI: 10.1002/anie.201502845
German Edition: DOI: 10.1002/ange.201502845

# Growth of Single-Layered Two-Dimensional Mesoporous Polymer/Carbon Films by Self-Assembly of Monomicelles at the Interfaces of Various Substrates**

*Yin Fang, Yingying Lv, Jing Tang, Hao Wu, Dingsi Jia, Dan Feng, Biao Kong, Yongcheng Wang, Ahmed A. Elzatahry, Daifallah Al-Dahyan, Qichun Zhang, Gengfeng Zheng,* and Dongyuan Zhao**

***Abstract:*** *Single-layered two-dimensional (2D) ultrathin mesoporous polymer/carbon films are grown by self-assembly of monomicelles at the interfaces of various substrates, which is a general and common modification strategy. These unconventional 2D mesoporous films possess only a single layer of mesopores, while the size of the thin films can grow up to inch size in the plane. Free-standing transparent mesoporous carbon ultrathin films, together with the ordered mesoporous structure on the substrates of different compositions (e.g. metal oxides, carbon) and morphologies (e.g. nanocubes, nanodiscs, flexible and patterned substrates) have been obtained. This strategy not only affords controllable hierarchical porous nanostructures, but also appends the easily modified and multifunctional properties of carbon to the primary substrate. By using this method, we have fabricated $Fe_2O_3$–mesoporous carbon photoelectrochemical biosensors, which show excellent sensitivity and selectivity for glutathione.*

Methods for constructing mesoscale subunits into 2D mesoporous frameworks remain in their infancy.[1–4] Mesoporous materials organize molecular components into periodic networks linked by covalent bonds, providing predictable structures with long-range order.[5–9] These materials show many desirable properties, including outstanding thermal stability, permanent porosity with a high surface area, and a tunable large pore size.[10–14] However, the unconfined self-assembly in the 3D space of the surfactants and mesoporous frameworks that are inherently cross-linked and insoluble, often results in bulk powders with 3D mesostructures.[3,15–18] The unavailability of 2D structures of these mesoporous materials limits their functions and applications, such as incorporation of π electron systems into ordered structures that are potentially ideal for optoelectronic devices.[2,19–24]

The development of facile and versatile strategies for thin-film and particle engineering is of immense scientific interest.[25–29] The existing method toolbox for functional modification of material surfaces includes self-assembled monolayer (SAM) formation, silane functionalization, layer-by-layer assembly, and genetically engineered surface-binding peptides.[26–28] Although widely implemented in research, these methods have limitations for widespread practical uses. In particular, the surface modification of periodic supermolecular thin films with complicated structures is still a great challenge. Until recently, the surface coating of 2D covalent organic frameworks (COFs)[2,19] has been reported. Nonetheless, the assembly of 2D mesoporous polymer/carbon thin films on the surface is highly difficult to be realized.[3,4] Moreover, none of feasible methods has been developed yet to realize the conformal coating of mesostructures on the substrates of different composition, size, shape, and structure.

In this work, we demonstrate a new surfactant-assisted hydrothermal approach for supermolecular self-assembly at the interface to grow 2D mesoporous carbon/polymer ultrathin films on various substrates. The 2D ultrathin films have only a single layer of mesopores (with a thickness of about 1 nm), while the size of the films can grow up to inch size on a plane. This strategy offers a general route for self-assembly of monomicelles at the interface of various kinds of substrates

[*] Dr. Y. Fang,[+] Dr. Y. Y. Lv,[+] J. Tang, H. Wu, D. S. Jia, Dr. D. Feng, B. Kong, Y. Wang, Prof. G. F. Zheng, Prof. D. Y. Zhao
Department of Chemistry, iChEM
Laboratory of Advanced Materials
Shanghai Key Laboratory of Molecular Catalysis and Innovative Materials, Fudan University
Shanghai 200433 (P.R. China)
E-mail: gfzheng@fudan.edu.cn
dyzhao@fudan.edu.cn
Homepage: http://www.mesogroup.fudan.edu.cn/
Dr. A. A. Elzatahry
Materials Science and Technology Program
College of Arts and Sciences, Qatar University
P.O. Box 2713, Doha (Qatar)
Prof. D. Al-Dahyan
Department of Chemistry, King Saud University
Riyadh 11451 (Saudi Arabia)
Prof. Q. Zhang
School of Materials Science and Engineering
Nanyang Technological University
Singapore 639798 (Singapore)
[+] These authors contributed equally to this work.

[**] This work was supported by the National Key Basic Research Program of China (grant number 2013CB934104), the NSF of China (grant numbers 21322311, 21473038, and 21210004), the Shanghai Leading Academic Discipline Project (B108), the Science and Technology Commission of Shanghai Municipality (grant numbers 14JC1400700, 14JC1490500, and 08DZ227 0500). The authors extend their appreciation to the Deanship of Scientific Research at King Saud University for funding the work through the research group project number RGP-227 and Delta Company Foundation.
Supporting information for this article is available on the WWW under http://dx.doi.org/10.1002/anie.201502845.

  

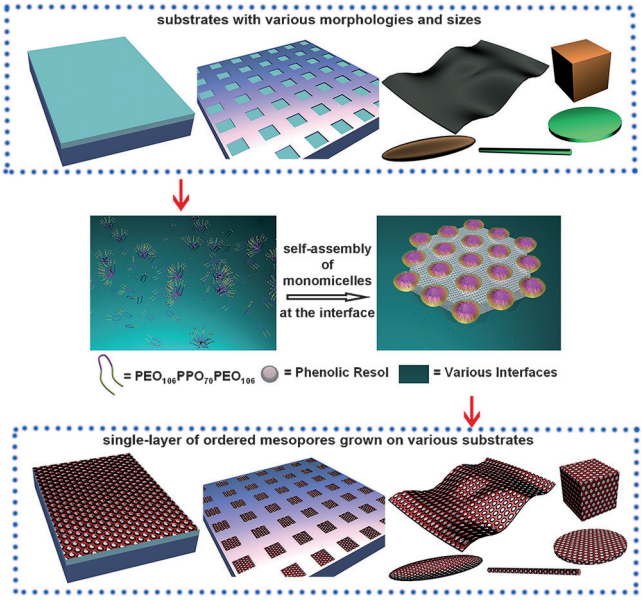


***Scheme 1.*** Interfacial self-assembly process of monomicelles to form single-layer mesoporous polymer/carbon thin films on various substrates.

with different morphologies and compositions (Scheme 1), such as nanocubes, nanodiscs, nanowires, nanorods, flexible surfaces, and patterned substrates by hydrothermal treatment. Furthermore, after peeled off from the substrates, free-standing 2D mesoporous ultrathin films can be formed. This strategy of single-layered mesoporous polymer/carbon surface growth not only enables constructing controllable porous hierarchical nanostructures, but also append the easily modified and multifunctional properties of carbon to the primary substrate, and thus may potentially serve as ideal candidates in a variety of applications. As a proof-of-concept, by using this method we have modified the surface properties of the optoelectronic devices by single-layer mesoporous carbon coating to fabricate efficient and sensitive photoelectrochemical biosensors.[30–32]

Single-layered 2D mesoporous polymer/carbon ultrathin films have been grown by supermolecular self-assembly of monomicelles at the interfaces of substrates under hydrothermal conditions (about 130 °C). Silicon wafers coated with a 50 nm thick layer of $Al_2O_3$ are employed as the substrate and surfactant monomicelles are employed as building blocks to assemble into ordered mesostructures at the interface (see the Experimental Section). 2D mesoporous polymer ultrathin films with an area from $1 \times 1$ cm$^2$ to one-quarter of a 3-inch silicon wafer have been grown on the substrates, indicating the possibility of continuous growth of large-size 2D mesostructures. After growing mesoporous nanostructures, the wafers still exhibit polished mirror-like surfaces, suggesting the ultrathin and homogeneous nature of the mesoporous carbon (Figure 1 a). In addition to homogeneous planar surface, the single layer of mesostructures has been grown

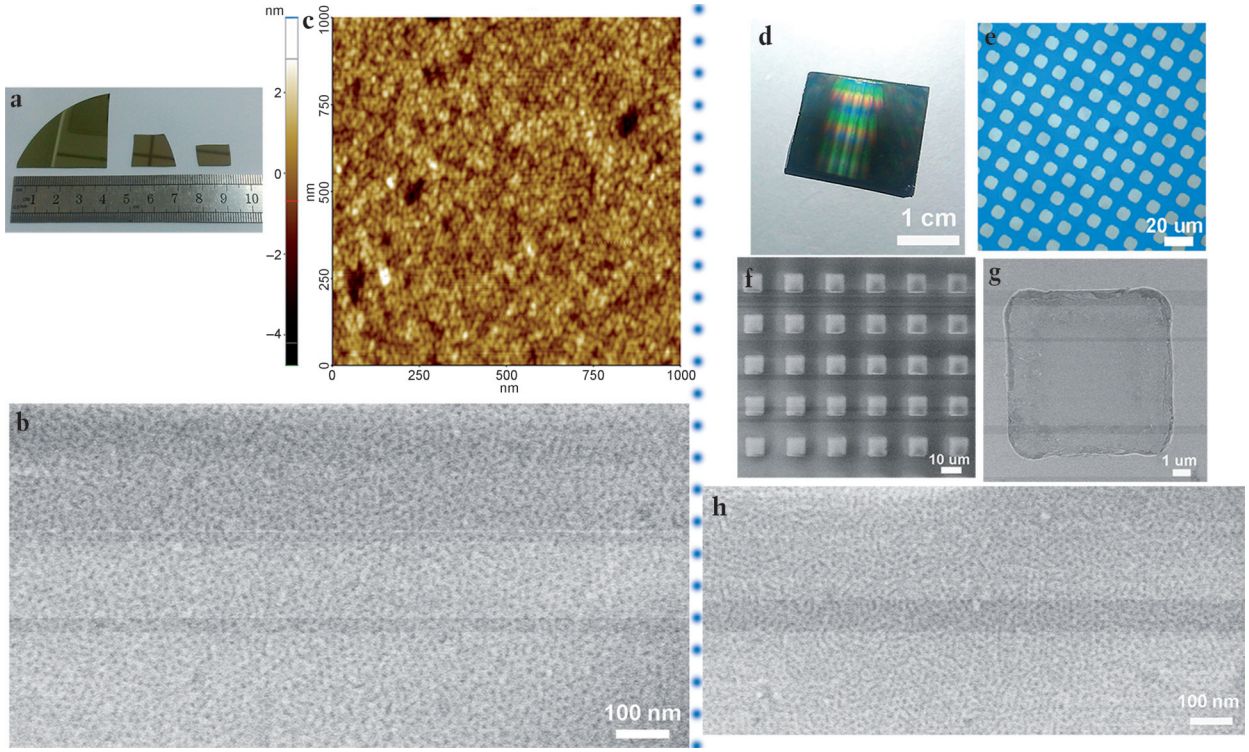


***Figure 1.*** Interfacial self-assembly process of monomicelles to form a single-layer mesoporous carbon thin film on a silicon wafer. a) Optical images of the large-scale mesostructures grown on silicon wafer surfaces. b) HR-SEM images of the ordered mesoporous carbon structures on a surface. c) AFM topography images of single-layer monomicellar carbon mesostructures on a silicon wafer. d,e) Optical images and f,g) SEM images of single-layer mesoporous carbon ultrathin films on the patterned silicon wafer, showing the square array-like patterned surface of the wafer. h) HR-SEM images of the ordered mesoporous structures on patterned surface.

on lithographically defined areas of patterned square arrays (see the Experiment Section), resulting in single-layered mesostructured carbon squares ($10 \times 10\ \mu m^2$; Figure 1 d–h). High-resolution scanning electron microscopy (HRSEM) images of the inch-scale plane show that before growth, the substrates do not have any features of mesopores (Figure S1a). After the growth of the single carbon layers, the patterned substrates display uniform mesopores with a size of about 9 nm and high orientation, indicating the ordered mesostructures of the carbon ultrathin films (Figure 1 b and Figure S1b). The periodic mesostructures are also displayed in AFM topography images (Figure 1 c and Figure S2). The dark area with a low elevation represents the mesopores, while the light area with a high elevation represents the carbon pore walls (Figure S2a). The existence of ordered mesostructures leads to the oriented alternation of dark and light areas, which are also shown by the depth shifts in the depth profile (Figure S2b).

The single layer of the 2D mesoporous carbon ultrathin films can be further peeled off from the silicon wafer and transferred to other substrates by a stamp transfer method (see the Experiment Section). Free-standing 2D mesoporous carbon ultrathin films are formed after the transfer (Figure 2 a), which exhibit unique properties compared to bulk 3D mesoporous materials. Normally, mesoporous carbon materials are excellent light absorber and thus always black in color. However, these unconventional ultrathin mesoporous carbon films are transparent, which allows for observing items or landscapes through the films (Figure 2 b,c). The transmittance of this single-layer material is detected to be over 85 % in the visible light wavelength (Figure 2 d), comparable to ultrathin graphene materials. Due to the different refractivity of the thin film and the water/air interface, the transparent single-layered mesoporous carbon ultrathin films can be directly observed by naked eyes. The thickness of the mesoporous carbon films measured from the AFM technique is about 1 nm (Figure 2 e), far smaller than the size of mesophase micelles, indicating that the ultrathin film is composed of a single layer of the mesoporous nanostructures.

The 2D mesoporous carbon ultrathin films can also be transferred onto a copper grid by the stamp transfer method (Figure 2 f,g). From some cracked parts, the ultrathin nanostructures are observed, further confirming the single-layered 2D structures (Figure 2 f,g). The thin films clearly display ordered mesostructures with uniform pore morphology filling in the whole domain size of the film. The average pore size is measured to be about 9 nm (Figure 2 h,i). No overlay of mesopores is observed in the ultrathin film, suggesting that these mesopores are closely packed on a single-layer plane. The distorted six-membered carbon rings arranged by carbon atoms can be seen in the high-resolution TEM (HRTEM) images, indicating the graphite nature of this thin carbon film (Figure S3).

The monomicelle interface self-assembly strategy has also been employed for flexible substrates. Reduced graphene oxide (rGO), is used as the initial substrate. After the surface coating, the materials maintain the morphology of 2D layered nanosheets of rGO in a large scale (Figure S4a), while the thickness is increased slightly compared to the initial rGO substrate (Figure S4b). The highly ordered mesopores are clearly observed on the surface of the whole layered rGO nanosheets (Figure 4 a,b), indicating the successful monomicelle interface self-assembly on rGO. Both faces of the 2D rGO are grown with 2D single-layered mesostructure, resulting in a sandwich-like 2D ultrathin film. TEM images demonstrate a 2D ultrathin film-like morphology of rGO coated with mesostructures in micrometer scale (Figure S4c,d). The ordered mesostructures filling in the whole domain size of the rGO are observed, with the average pore size of about 9 nm (Figure S4d). The sandwich-like morphology can be observed on the edge of the rGO in the TEM

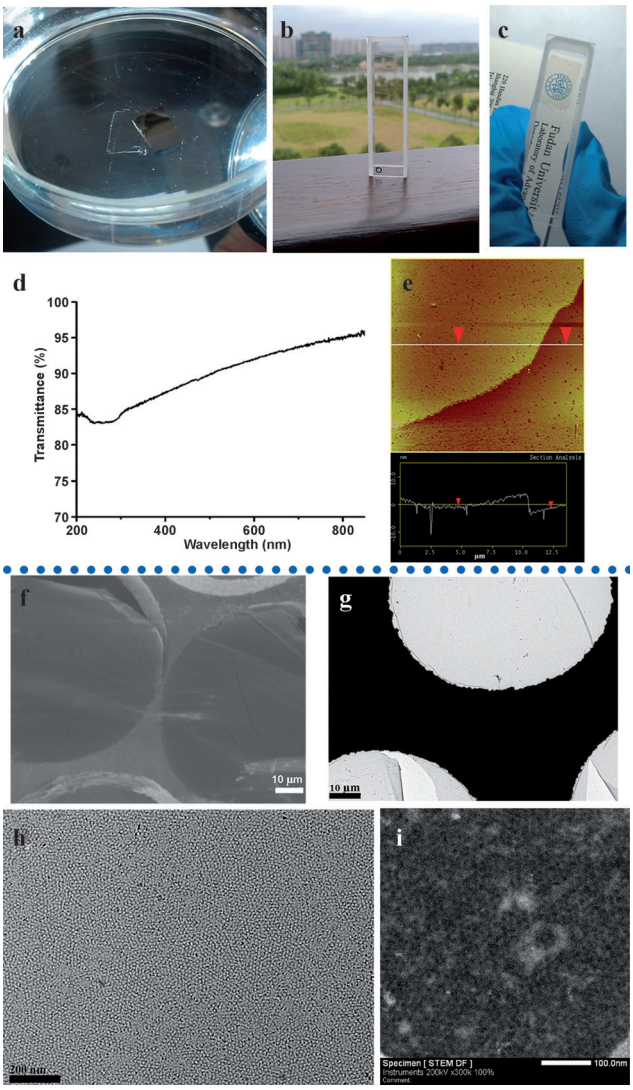


***Figure 2.*** a) Optical images of the free-standing ultrathin film for 2D mesoporous single layer floating on the water phase after it is peeled off from the substrate. b,c) Optical images of the 2D mesoporous ultrathin film adhered to a cuvette. Graphs or landscapes could be clearly watched through the ultrathin film. d) The transmittance curves of the free-standing mesoporous carbon ultrathin film. e) AFM images of the ultrathin film, and the height of it. f) SEM (scale bar = 10 μm) and g) TEM (scale bar = 10 μm) images of the 2D single-layer mesoporous carbon ultrathin films transferred onto the copper grid. h) TEM (scale bar = 200 nm) and i) STEM (scale bar = 100 nm) images of the large-domain-sized ordered mesostructures on the ultrathin film.

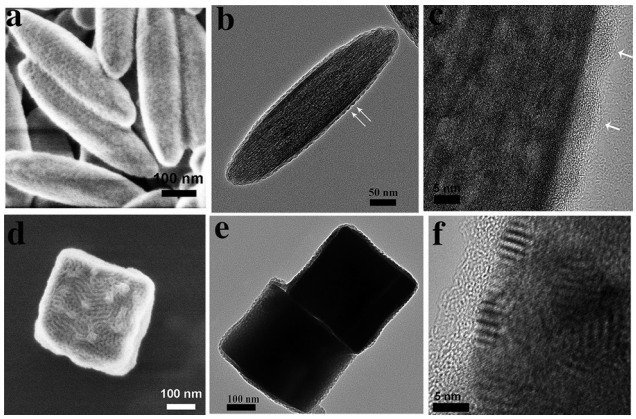


***Figure 3.*** a) SEM (scale bar = 100 nm) and b) TEM (scale bar = 50 nm) and c) HR-TEM (scale bar = 5 nm) images of the FeOOH nanoellipsoid surface modified with single-layer mesoporous carbonaceous nanostructures. d) SEM (scale bar = 100 nm) and e) TEM (scale bar = 100 nm) and f) HR-TEM (scale bar = 5 nm) images of $Cu_2O$ nanocubes modified with a single-layer mesoporous ultrathin nanostructure by using an interfacial self-assembly process of monomicelles.

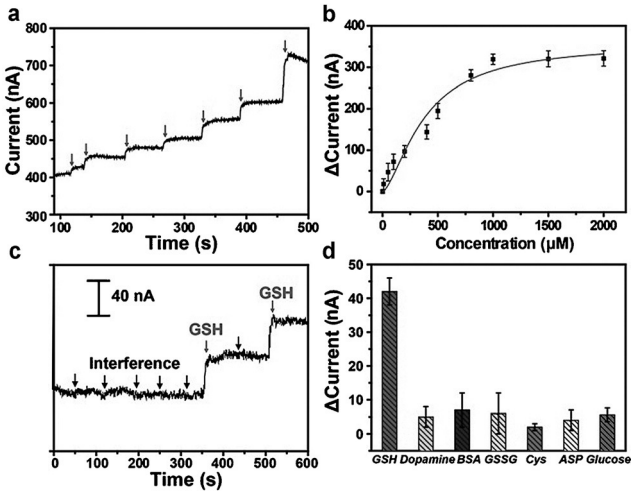


***Figure 4.*** a) Photocurrent versus time plot of the Fe2O3-single-layered mesoporous carbon–hemin nanorod biosensor for the addition of GSH at 0 V versus Ag/AgCl under sun light illumination. Each arrow indicates the addition of GSH into PBS buffer, with a final GSH concentration increase of 1.6 μm (about 1 mm each time). b) Summary of the sensing signal versus GSH concentration. c) Photocurrent versus time plot on the Fe2O3-single-layered mesoporous carbon–hemin nanorod biosensor for continuous addition of GSH (with a final concentration increase of 50 μm at a time), and other interference molecules (with a final concentration increase of 50 μm each time), designated by the arrows. d) Summary of the photocurrent alteration of the Fe2O3-single-layered mesoporous carbon–hemin nanorod biosensors at the appearance of the GSH analogs. The sizes of the active sensor area for (a–d) are approximately 0.02–0.06 cm2.

images. The dark slice is the section of the rGO, while two sides along the section is the profile of mesopores.

This interfacial self-assembly method of monomicelles has further been used to realize the surface growth of nanosized materials with different morphologies. After surface modification, the ellipsoid FeOOH nanoparticles (about 500 nm in length, 100 nm in width, Figure S5) clearly exhibit ordered mesopores on the surface with a pore size of about 9 nm (Figure 3a). TEM images reveal that the nanostructures of the ellipsoids are similar to the core–shell structure, where a tiny layer of 1–3 nm is grown on the FeOOH nanoparticles (Figure 3b and Figure S6). The outside layer has a hackled shape, where the concave parts represent the mesopore, and the convex parts are for the pore wall (Figure 3b,c the white arrows). The outside layer shows the profiles of the single layer of the mesopores. Controlled growth of single-layer mesopores modified on a nanoellipsoid surface is shown for the first time. In addition, the growth of mesoporous single layer has further been shown on the surface of cubic-like $Cu_2O$ (Figure 3d–f), disc-like $Ni(OH)_2$ (Figure S7a–c), 1D nanowires with several micrometers in length (Figure S8), and nanoparticles with a diameter smaller than 50 nm (Figure S9). The mechanism of the formation of mesoporous monolayer thin films is proposed as the controlled assembly of monomicelles and a heterogeneous nucleation process on the substrate surface. The monomicelles are rich in phenolic hydroxy groups, which lead to the strong interaction between the composite monomicelles and the substrate surface.

Our synthetic strategy also enables in situ interfacial modification of nanorod array devices. The $Fe_2O_3$ nanorod array is selected as a proof-of-concept because of its attractive light absorption property for photoelectrochemical catalysis. Initially, the surface of the $Fe_2O_3$ nanorods (about 1 μm in length, 200 nm in width) is smooth (Figure S10a,b). After the carbon ultrathin film growth, a single layer of ordered mesopores with a pore size of about 9 nm is found to uniformly cover the whole surface of each $Fe_2O_3$ nanorod (Figure S10c,d). TEM images also show the core–shell nanostructures of the nanorods. The outside layer shows the hackled shape of the single mesopore layers (Figure S10e,f), further demonstrating the successful growth of mesostructured monomicelles. The single layer of ordered mesoporous carbon is highly conductive for enhancing the charge transport of $Fe_2O_3$ and remains transparent and thus does not affect the penetration and adsorption of solar light. The photocurrent density at 0 V versus Ag/AgCl for the surface-modified $Fe_2O_3$–mesoporous carbon nanorods is about 0.5 mA $cm^{-2}$, which is 1.5 times higher than that for pristine $Fe_2O_3$ nanorod arrays (ca. 0.35 mA $cm^{-2}$; Figure S10g,h).

After grafted with hemin on the $Fe_2O_3$-single layered mesoporous carbon nanorods, the device is found to be an excellent glutathione (GSH) sensor. GSH is a significant thiolated tripeptide and endogenous antioxidant that is ubiquitous in the intracellular environment.[33] The hemin molecules modified on the surface can specifically combine with GSH, which is used as the electron donor to the photogenerated holes of the excited state of hemin.

The GSH level in an electrolyte can be tested as the photoelectrochemical cell (PEC) sensing signal by a time-dependent photocurrent measurement. By continuous additions of GSH at intervals where the concentration gradually increases, the $Fe_2O_3$-single-layered mesoporous carbon–hemin nanorod electrode reaches equilibrium within tens of seconds (Figure 4a). The conductance change with different GSH concentrations demonstrates a linear range of 1.6–

  

500 μM (Figure 4b). In comparison, the addition of different amino acids or common chemical/biological interferences only gives rise to a much smaller or negligible photocurrent change (Figure 4c). The sensing activity is comparable with previous work,[33] even different photoelectrochemical sensor materials were used. More importantly, the sensing activity is notably improved after the growth of the single-layered mesoporous carbon film. The selectivity of the $Fe_2O_3$-single-layered mesoporous carbon–hemin nanorod-based PEC sensor is further interrogated by measuring the responses from various analogs or interferences, including bovine serum albumin (BSA), cysteine (Cys), dopamine, aspartic acid (ASP), glucose, and GSSG concentrations of 50 μM. All these interference solutions show a much smaller or negligible signal compared to the GSH solution with similar concentrations (Figure 4d), indicating the high selectivity.

In conclusion, we have demonstrated an interfacial self-assembly method of monomicelles under hydrothermal conditions to grow ultrathin single-layered 2D mesoporous polymer and carbon films. This method is a general modification strategy for a large variety of substrate surfaces, and can be used to synthesize thin films from inch size to nanometer scale and on different surface compositions (e.g. metal oxides, carbon) and morphologies, including nanocubes, nanodiscs, nanowires, nanorods, flexible surfaces and on patterned substrates. After peeling off from the substrate of silicon wafer, a free-standing transparent mesoporous carbon ultrathin film can be obtained. This monolayered ultrathin film with the thickness of about 1 nm is only composed of one single layer of about 9 nm mesopores and transparent in visible light wavelength. By using this general interfacial self-assembly method of monomicelles, an $Fe_2O_3$-mesoporous carbon photoelectrochemical biosensor is obtained, showing excellent GSH sensing activity and selectivity. Attributed to their highly ordered mesostructures, transparent properties, and excellent electrical conductivity, these 2D mesoporous carbon ultrathin films may be further explored and find unconventional applications in both renewable energy and life sciences.

**Keywords:** biosensors · carbon · mesoporous materials · nanomaterials · thin films

**How to cite:** *Angew. Chem. Int. Ed.* **2015**, *54*, 8425–8429
*Angew. Chem.* **2015**, *127*, 8545–8549

[1] M. S. Xu, T. Liang, M. M. Shi, H. Z. Chen, *Chem. Rev.* **2013**, *113*, 3766–3798.
[2] J. W. Colson, W. R. Dichtel, *Nat. Chem.* **2013**, *5*, 453–465.
[3] Y. Fang, Y. Y. Lv, R. C. Che, H. Y. Wu, X. H. Zhang, D. Gu, G. F. Zheng, D. Y. Zhao, *J. Am. Chem. Soc.* **2013**, *135*, 1524–1530.
[4] J. J. Duan, S. Chen, M. Jaroniec, S. Z. Qiao, *ACS Nano* **2015**, *9*, 931–940.
[5] Y. Wan, D. Y. Zhao, *Chem. Rev.* **2007**, *107*, 2821–2860.
[6] Y. F. Shi, Y. Wan, D. Y. Zhao, *Chem. Soc. Rev.* **2011**, *40*, 3854–3878.
[7] T. Y. Ma, L. Liu, Z. Y. Yuan, *Chem. Soc. Rev.* **2013**, *42*, 3977–4003.
[8] C. D. Liang, Z. J. Li, S. Dai, *Angew. Chem. Int. Ed.* **2008**, *47*, 3696–3717; *Angew. Chem.* **2008**, *120*, 3754–3776.
[9] N. D. Petkovich, A. Stein, *Chem. Soc. Rev.* **2013**, *42*, 3721–3739.
[10] P. F. Zhang, H. Y. Li, G. M. Veith, S. Dai, *Adv. Mater.* **2015**, *27*, 234–239.
[11] X. Du, L. Xiong, S. Dai, F. Kleitz, S. Z. Qiao, *Adv. Funct. Mater.* **2014**, *24*, 7627–7637.
[12] G. P. Hao, Z. Y. Jin, Q. Sun, X. Q. Zhang, J. T. Zhang, A. H. Lu, *Energy Environ. Sci.* **2013**, *6*, 3740–3747.
[13] G. P. Hao, W. C. Li, D. Qian, G. H. Wang, W. P. Zhang, T. Zhang, A. Q. Wang, F. Schuth, H. J. Bongard, A. H. Lu, *J. Am. Chem. Soc.* **2011**, *133*, 11378–11388.
[14] J. Liang, X. Du, C. Gibson, X. W. Du, S. Z. Qiao, *Adv. Mater.* **2013**, *25*, 6226–6231.
[15] Y. Fang, G. F. Zheng, J. P. Yang, H. S. Tang, Y. F. Zhang, B. Kong, Y. Y. Lv, C. J. Xu, A. M. Asiri, J. Zi, F. Zhang, D. Y. Zhao, *Angew. Chem. Int. Ed.* **2014**, *53*, 5366–5370; *Angew. Chem.* **2014**, *126*, 5470–5474.
[16] A. H. Lu, G. P. Hao, Q. Sun, X. Q. Zhang, W. C. Li, *Macromol. Chem. Phys.* **2012**, *213*, 1107–1131.
[17] A. H. Lu, W. C. Li, G. P. Hao, B. Spliethoff, H. J. Bongard, B. B. Schaack, F. Schuth, *Angew. Chem. Int. Ed.* **2010**, *49*, 1615–1618; *Angew. Chem.* **2010**, *122*, 1659–1662.
[18] J. Tang, J. Liu, C. Li, Y. Li, M. O. Tade, S. Dai, Y. Yamauchi, *Angew. Chem. Int. Ed.* **2015**, *54*, 588–593; *Angew. Chem.* **2015**, *127*, 598–603.
[19] J. W. Colson, A. R. Woll, A. Mukherjee, M. P. Levendorf, E. L. Spitler, V. B. Shields, M. G. Spencer, J. Park, W. R. Dichtel, *Science* **2011**, *332*, 228–231.
[20] J. F. Dienstmaier, A. M. Gigler, A. J. Goetz, P. Knochel, T. Bein, A. Lyapin, S. Reichlmaier, W. M. Heckl, M. Lackinger, *ACS Nano* **2011**, *5*, 9737–9745.
[21] S. A. Claridge, W. S. Liao, J. C. Thomas, Y. Zhao, H. H. Cao, S. Cheunkar, A. C. Serino, A. M. Andrews, P. S. Weiss, *Chem. Soc. Rev.* **2013**, *42*, 2725–2745.
[22] S. B. Yang, X. L. Feng, L. Wang, K. Tang, J. Maier, K. Mullen, *Angew. Chem. Int. Ed.* **2010**, *49*, 4795–4799; *Angew. Chem.* **2010**, *122*, 4905–4909.
[23] Z. M. Wang, W. Wang, N. Coombs, N. Soheilnia, G. A. Ozin, *ACS Nano* **2010**, *4*, 7437–7450.
[24] D. H. Wang, R. Kou, D. W. Choi, Z. G. Yang, Z. M. Nie, J. Li, L. V. Saraf, D. H. Hu, J. G. Zhang, G. L. Graff, J. Liu, M. A. Pope, I. A. Aksay, *ACS Nano* **2010**, *4*, 1587–1595.
[25] H. L. Wang, H. J. Dai, *Chem. Soc. Rev.* **2013**, *42*, 3088–3113.
[26] H. Lee, S. M. Dellatore, W. M. Miller, P. B. Messersmith, *Science* **2007**, *318*, 426–430.
[27] H. Ejima, J. J. Richardson, K. Liang, J. P. Best, M. P. van Koeverden, G. K. Such, J. Cui, F. Caruso, *Science* **2013**, *341*, 154–157.
[28] D. H. Kim, J. Viventi, J. J. Amsden, J. L. Xiao, L. Vigeland, Y. S. Kim, J. A. Blanco, B. Panilaitis, E. S. Frechette, D. Contreras, D. L. Kaplan, F. G. Omenetto, Y. G. Huang, K. C. Hwang, M. R. Zakin, B. Litt, J. A. Rogers, *Nat. Mater.* **2010**, *9*, 511–517.
[29] K. S. Kim, Y. Zhao, H. Jang, S. Y. Lee, J. M. Kim, J. H. Ahn, P. Kim, J. Y. Choi, B. H. Hong, *Nature* **2009**, *457*, 706–710.
[30] B. Z. Tian, T. Cohen-Karni, Q. Qing, X. J. Duan, P. Xie, C. M. Lieber, *Science* **2010**, *329*, 830–834.
[31] B. Z. Tian, C. M. Lieber, *Annu. Rev. Anal. Chem.* **2013**, *6*, 31–51.
[32] B. Z. Tian, J. Liu, T. Dvir, L. H. Jin, J. H. Tsui, Q. Qing, Z. G. Suo, R. Langer, D. S. Kohane, C. M. Lieber, *Nat. Mater.* **2012**, *11*, 986–994.
[33] J. Tang, B. Kong, Y. C. Wang, M. Xu, Y. L. Wang, H. Wu, G. F. Zheng, *Nano Lett.* **2013**, *13*, 5350–5354.

Received: March 27, 2015
Revised: April 25, 2015
Published online: June 18, 2015

  